Journal of Materials Chemistry B

PAPER

View Article Online
View Journal | View Issue

Cite this: J. Mater. Chem. B, 2015, 3, 849

On the antitumor properties of biomedical magnesium metal

Yangmei Chen,[ab] Ming Xiao,[ab] Huan Zhao[ab] and Bangcheng Yang*[ab]

H_2 is a therapeutic agent for tumors because it could scavenge free radicals, which is one of the causes for this disease in the human body. Biomedical magnesium (Mg) could release H_2 in the biodegradation process, thus it might have antitumor properties. In this study, Mg metal (P-Mg) was subjected to anodic oxidation plus heat treatment to get AO-HT-Mg covered with MgO. In SBF experiments AO-HT-Mg showed bioactivity as it could induce calcium phosphate deposition. The MgO layer played a protective role in the biodegradation process and controlled the H_2 releasing rate. In MRMT-1 rat breast carcinoma cell culture experiments, both P-Mg and AO-HT-Mg could inhibit free radical expression in the cells, and AO-HT-Mg showed higher inhibiting ability. In the animal experiments with 72 mice divided into 4 groups, both P-Mg and AO-HT-Mg could inhibit tumor growth. After implantation in the animals, P-Mg showed higher inhibiting ability at the initial stage, and AO-HT-Mg showed higher inhibiting ability after 26 days. The tumor inhibiting properties depended on H_2 releasing rates. The results confirm Mg metal has antitumor properties *in vivo*, and it is possible to optimize its antitumor properties by surface modification.

Received 27th August 2014
Accepted 11th November 2014

DOI: 10.1039/c4tb01421a

www.rsc.org/MaterialsB

1 Introduction

Magnesium (Mg) metal has been widely reported to be a potential biomaterial for tissue replacement and regeneration, especially for bony tissue and the cardiovascular system, because of its biodegradation properties *in vivo*.[1–3] After Mg metal is implanted in the body, it will be absorbed and replaced by the regenerative tissues. During biodegradation, by-products including Mg^{2+} and H_2 will be produced and have a great influence on the tissue response *in situ*.[4–6] It has been reported that H_2 would induce fracture of the bone in the bony tissue and destroy vascular stents in the cardiovascular system.[7,8] Thus, the topics about biomedical Mg research in the past decades mainly focused on its biodegradation to prevent the negative effects of H_2.

In recent years, it has been reported that H_2 is a therapeutic agent for free radical related diseases, including cancers and senile diseases.[9–12] H_2 could scavenge the free radicals, especially the reactive hydroxyl radicals ($^{\cdot}OH$) and peroxynitrite ($ONOO^-$), which are the causes for these diseases.[13] In a research of Ohsawa and colleagues, they reported that H_2 scavenged the reactive hydroxyl radicals according to the following reaction (1):[14]

$$H_2 + {}^{\cdot}OH \rightarrow H_2O + H^{\cdot} \quad (1)$$

After the free radicals were scavenged, the diseases associated with them were significantly restrained.

As the biomedical Mg could release H_2 during the biodegradation, it is logical to assume that Mg metal is a potential material with therapeutic properties to inhibit the free radical related diseases. Thus, in our previous study, we proposed that Mg might be a potential biomaterial with antitumor properties, and we found H_2 released from Mg was effective for scavenging free radicals in the Fenton reaction system and osteosarcoma cells.[15]

In order to confirm the antitumor properties of Mg metal in detail, we studied the antitumor properties of biomedical Mg *in vivo* in this study. Anodic oxidation plus heat treatment surface modification method was employed to control the biodegradation of Mg.

2 Experimental section

2.1 Surface modification and characterization of Mg metal

Commercial pure Mg metal (P-Mg, 99.95%) was used for this study. Mg plates (10 mm × 10 mm × 1 mm) were polished with 400 grit, 800 grit, and 1000 grit sandpaper, and then ultrasonically cleaned individually three times with acetone, ethanol, and distilled water in turn. The as-received plates were subjected to anodic oxidation plus heat treatment according to the method described in the ref. 16. The anodic oxidation treatment was performed at a galvanostatic model of 0.05 A in 1 L KOH solution (1 M in concentration) for 30 min at room temperature. The samples were further heat treated at 500 °C for 1 h to

[a]Engineering Research Center in Biomaterials, Sichuan University, Chengdu, 610064, China. E-mail: yangbchengc@126.com
[b]National Engineering Research Center for Biomaterials, Chengdu, 610064, China

change the $Mg(OH)_2$ to MgO on the surface. We defined the as-received metal after this modification as AO-HT-Mg. Both P-Mg and AO-HT-Mg were analyzed with X-ray diffraction (XRD, DX-1000 X-ray diffractometer) and scanning electron microscopy (SEM, HITACHI-S4800, Japan) to characterize the surface changes of Mg metals after the treatments. XRD analysis was carried out with Cu Kα radiation working with 40 kV and 25 mA. The 2θ range varies from 20° to 80° at a scanning rate of 0.02° s^{-1}. SEM observation was performed with an accelerating voltage of 30 kV.

2.2 Biodegradation of Mg metals *in vitro*

In order to study the bioactivity of P-Mg and AO-HT-Mg, they were soaked in 10 mL of simulated body fluid (SBF) at 37 °C for 24 h, and then they were analyzed with XRD and SEM. SBF was prepared by dissolving NaCl, $NaHCO_3$, KCl, $K_2HPO_4 \cdot 3H_2O$, $MgCl_2 \cdot 6H_2O$, $CaCl_2 \cdot 2H_2O$, and Na_2SO_4 in distilled water and adjusting the pH value to 7.4 with 1 M HCl and Tris, according to the method of Kokubo.[17] In order to investigate the biodegradation of both the metals, the metals were soaked in 50 mL SBF for 85 h, according to the requirement of ASTMG31-72. The pH values of the solutions and the amounts of H_2 released from the degradation were monitored every 3 h. The pH value was detected by a pH meter (Mettle Toledo, FE20, Swiss). For each time point, at least three samples were studied to get the average data.

2.3 *In vitro* antitumor properties of Mg metals

2.3.1 Breast carcinoma cell culture. In order to study the antitumor properties of Mg *in vitro*, MRMT-1 rat breast carcinoma cells at the 7th passage were employed to study the effects of Mg on the free radicals expression in the cells. MRMT-1 cells were cultured in Dulbecco's modified Eagle's medium (DMEM, Gibco, USA) containing 10% newborn calf serum and 1% antibiotic under 5% CO_2 atmosphere at 37 °C. After P-Mg and AO-HT-Mg were subjected to radiation sterilization for 21 h at 25 KGy (FJX424, Co_{60} γ rays), specimens were placed in 12-well plates, and 3 mL medium was introduced into each well to balance the surface for 24 h, according to our previous study.[15] During the balance procedure, the medium was replaced with fresh medium every 4 h. The purpose of balancing the surface was to make the surface suitable for cell survival. After the balanced metals were dried with cold air, they were placed into 24-well plates again, and 2 mL cell suspension (1.5×10^5 cells per mL) was added onto the metal plates to culture for 1, 2 and 3 days. A group of wells without any material was also cultured with cells, which were set as controls. The medium was replaced every 24 h during the culture. At 1, 2 and 3 days, the cell-cultured samples were taken out of the culture plate and washed two times with PBS. Then, the cells were stained with 5 μg mL^{-1} fluorescein diacetate for CLSM (Leica SP5, Germany) analysis to investigate their attachment and growth on the metals.

2.3.2 Detection of free radicals in the cell. ROS Assay Kit (Beyotime, China) was used to detect the levels of free radicals in MRMT-1 cultured on metal surfaces and blank wells. At 1, 2 and 3 days, the culture medium in 24-well plates was removed, and 300 μL 0.25% trypsin/1 mM EDTA solution was added into each well and swirled to cover the entire sample. Then, 1 mL serum-free medium was added to harvest the cells from the plate. The cells were transferred to a conical tube and centrifuged for 5 min (1200 rpm) at room temperature to collect the cells. After the supernatant was discarded, dichlorofluorescein diacetate (DCFH-DA) diluted to 1000 times with serum-free medium was placed into the conical tube for 30 min incubation in the oscillator at 37 °C. DCFH-DA is an uncharged, cell permeable fluorescent probe. Inside the cells DCFH-DA is cleaved by nonspecific esterases to form DCFH, which is oxidized to the fluorescent compound 2′,7′-dichlorofluorescein (DCF) in the presence of ROS. The DCFH-DA supernatant was removed from the conical tube by centrifuging, and the cells were washed three times with serum-free medium to remove the residual DCFH-DA. Finally, the average content of free radicals in a single cell was measured at 488 nm (excitation wavelength) and 525 nm (emission wavelength) by flow cytometry assay (FCA, BECKMAN, Cytomic Fc500. America).

2.4 *In vivo* antitumor properties of Mg metal

2.4.1 Animal experiment. In order to investigate the antitumor properties of Mg metals *in vivo*, 100 μL 4T1/Luc cells (1×10^7 cells per mL) was subcutaneously injected into an 8 week-old female BALB/c mouse (about 20 g in weight, Sichuan University) to prepare a transplantable tumor *in situ*. During the animal experiments, the animals were randomly divided into 4 groups with 18 mice in each group. Three groups of mice were anaesthetized with an intraperitoneal injection of 1% sodium pentobarbital. The back skin was shaved and disinfected with 75% ethanol. Two groups among them had the back muscles exposed after the skin incision. P-Mg and AO-HT-Mg were subcutaneously implanted in the animals and fixed on the muscles by sutures. After the wounds were closed, both groups of mice were subcutaneously injected with 4T1/Luc cells just near the metals. In the meantime, another anaesthetized group of mice without implants were also subcutaneously injected with 4T1/Luc cells as a control group. The group without any surgery was used as a blank group.

These experiments were conducted in accordance with the Guidelines for Animal Experimentation (National Engineering Research Center for Biomaterial, Sichuan University) regarding the care and use of animals in the experimental procedures, and the experiments have been approved by the institutional committee of National Engineering Research Center for Biomaterial, Sichuan University.

2.4.2 General observation. After the operation, the wound cicatrisation state of the animals was observed. After 7 days, tumor volume was measured every 3 or 4 days. The sizes of tumors were monitored with the following method (2), which had been widely used in ref. 18–20.

$$S = W^2 \times L/2 \quad (2)$$

S, *W* and *L* are the size, width, and length of tumor, respectively. The tumor growth rate was calculated with the sizes of the tumors.

2.4.3 *In vivo* imaging analysis. At 10, 20 and 30 days after the operation, the animals with tumors were intraperitoneally injected with 10 μL g^{-1} D-luciferin potassium salt (15 mg mL^{-1} in DPBS, Fanbo Biochemical, China). Ten minutes later, the animals were anaesthetized with sodium pentobarbital for the analysis with an *in vivo* imaging system (Maestro Ex Pro System, USA).

2.4.4 Malondialdehyde evaluation. At 10, 20 and 30 days after the operation, six animals of each group were sacrificed at every time point. The blood of the animals was collected, and the malondialdehyde (MDA) in serum was analyzed with mouse MDA ELISA Kit (R&D, USA). The operation of analysis procedure for MDA was according to the instruction of the kit. MDA level is a characteristic factor for ROS in serum. Higher ROS would result in higher MDA level in serum.[21]

2.4.5 Histological evaluation. After the animals were sacrificed, the tumors induced by 4T1/Luc cells were collected. The weights of the tumors were analyzed with an electronic balance. The tumors were fixed with 4% paraformaldehyde with pH value 7.4 for 24 h, dehydrated in gradient alcohols (70, 80, 90, 95, and 100%), and then embedded in paraffin. After the tumor was cut into sections with the thicknesses of 3 μm, it was stained with hematoxylin and eosin (HE) and observed under an optical microscope.

2.5 Statistical analysis

The results were statistically studied with SPSS11.0 software, and the corresponding *p*-values were considered to be significant at values less than 0.05. All the statistical analysis was performed with at least three samples for each single experiment.

3 Results

3.1 Mg metal surface characterization

XRD and SEM were used to characterize the surface structures of P-Mg and AO-HT-Mg. The SEM images (Fig. 1(A) and (B)) showed the P-Mg had a smooth surface, and the anodic oxidation plus heat treatment made the metal surface porous. From the XRD spectra (Fig. 1(C)), it was clear that only peaks of Mg could be found in P-Mg. For AO-HT-Mg, peaks for MgO appeared, as well as peaks of Mg. It indicated that the AO-HT-Mg was covered with a layer of MgO. In a previous study, it had been proved that $Mg(OH)_2$ would be formed on the surface by the anodic oxidation treatment (3).[22] MgO on the metal surface was formed by the decomposition of $Mg(OH)_2$ during the heat treatment (4).

$$Mg + H_2O \rightarrow Mg(OH)_2 + H_2\uparrow \quad (3)$$

$$Mg(OH)_2 \rightarrow MgO + H_2O\uparrow \quad (4)$$

The escaping of water vapor during the heat treatment would cause the porous structure of MgO.

3.2 Biodegradation of Mg metal

In order to examine the mineralization ability of modified samples, P-Mg and AO-HT-Mg were soaked in SBF for 24 h and presented by the SEM images and XRD spectra (Fig. 2). It was clear that AO-HT-Mg was covered by a layer of mineral (Fig. 2(A) and (B)). Some cracks appeared in the mineral. It indicated that mineral deposition happened on its surface during the biodegradation procedure in SBF. Only some corrosion pits could be found on P-Mg. The XRD spectra (Fig. 2(C)) showed that peaks of both Mg and $Ca_2P_2O_7$ appeared on the surface of AO-HT-Mg, and the peaks of MgO disappeared in the spectra of AO-HT-Mg after it was soaked in SBF for 24 h. Only the peaks of Mg and $Mg(OH)_2$ could be observed in the spectrum of P-Mg after it was soaked in SBF for 24 h. It also showed that the crystallinity of P-Mg surface decreased after the SBF soaking. It indicated a reaction between P-Mg and water. The formation of calcium phosphate on the AO-HT-Mg indicated its bioactivity in a biological environment. $Ca_2P_2O_7$ is the intermediate phase for apatite which is essential for a bioactive bonding between the biomaterials and bone. The porous surface structure of AO-HT-Mg could provide many more nucleation sites, which might be beneficial for the formation of calcium phosphate in SBF.

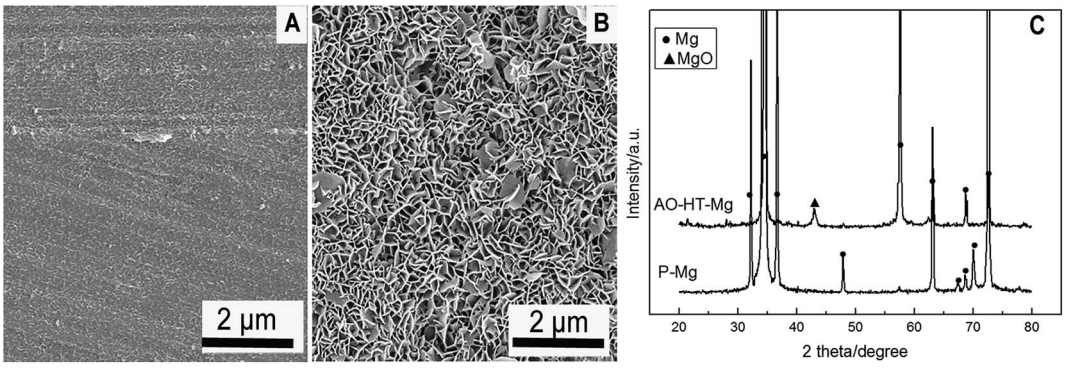

Fig. 1 The structures of P-Mg and AO-HT-Mg characterized by SEM (A and B, respectively) and XRD (C). (P-Mg: untreated Mg; AO-HT-Mg: Mg treated by anodic oxidation plus heat treatment).

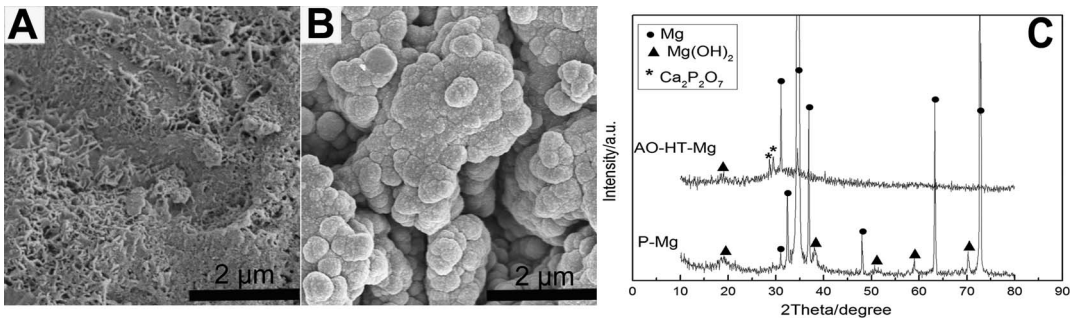

Fig. 2 The structures of P-Mg and AO-HT-Mg immersed in SBF for 24 h characterized by SEM (A and B) and XRD (C).

Immersion corrosion testing of Mg metals showed that the AO-HT-Mg presented the stronger ability to resist corrosion (Fig. 3). For the SBF soaked with P-Mg (Fig. 3(A)), the pH value steadily increased from 7.4 to 8.2 in the initial 30 h. After that it sharply increased to 9.8 in 15 h, and then the pH value became stable. For the SBF soaked with AO-HT-Mg (Fig. 3(A)), the pH value steadily increased from 7.4 to 8.5 after it was soaked with AO-HT-Mg for 85 h. The pH value of the SBF soaked with P-Mg was higher than that of AO-HT-Mg. It is well known that $Mg(OH)_2$, which is the product of Mg degradation, would increase the pH value of SBF. This result indicated that the degradation of AO-HT-Mg was slower compared to P-Mg. The anodic oxidation plus heat treatment was an effective method to control the biodegradation of Mg metal. It is obvious that the H_2 releasing rate of AO-HT-Mg was considerably slower than that of the P-Mg (Fig. 3(B)). It is logical to realize H_2 control releasing by controlling the biodegradation of Mg through the surface modification.

MgO formed on Mg metal by anodic oxidation plus heat treatment provided a protective role for metal degradation. Additionally, calcium phosphate formed on the surface in SBF might also provide a protective role for the metal.

3.3 *In vitro* antitumor properties of Mg metals

In the studies of our laboratory, we have confirmed that the cells could not survive on the Mg metal if it had not been subjected to balancing in cell culture medium, in which the high pH in the medium resulting from the biodegradation made the environment unsuitable for cell survival.[15] After the balancing procedure in medium for 24 h, a biomimetic coating formed on both surfaces (Fig. 4), and the pH value of the medium decreased to 8.2. It is reported that the biomimetic coating formed in the medium could protect Mg metal.[23] It is obvious that the protective role of the biomimetic coating could not change the biodegradation trends for both Mg metals, although it is an effective method to make the surfaces of both Mg metals suitable for cell survival.

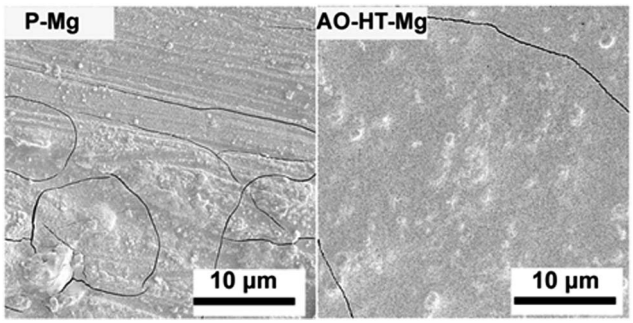

Fig. 4 SEM micrographs of P-Mg and AO-HT-Mg samples immersed in Dulbecco's modified Eagle's medium (DMEM) for 24 h.

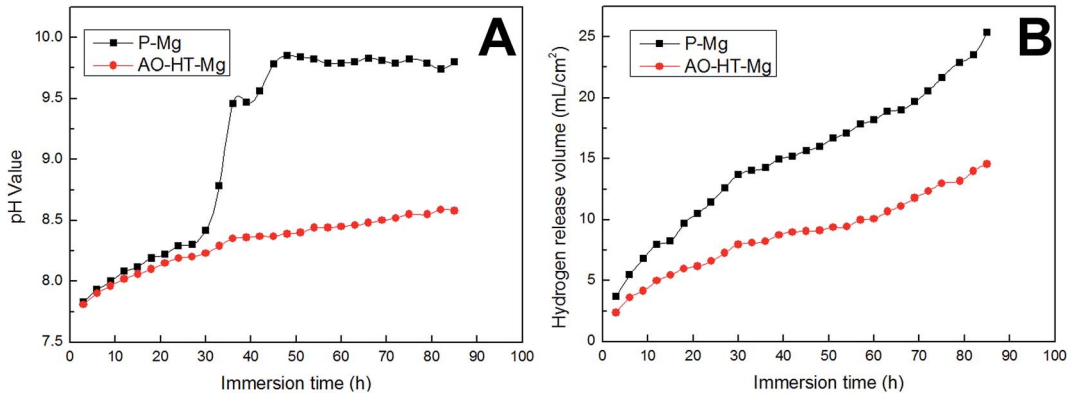

Fig. 3 The pH changes (A) and hydrogen releasing volumes (B) of P-Mg and AO-HT-Mg as a function of immersion time in SBF.

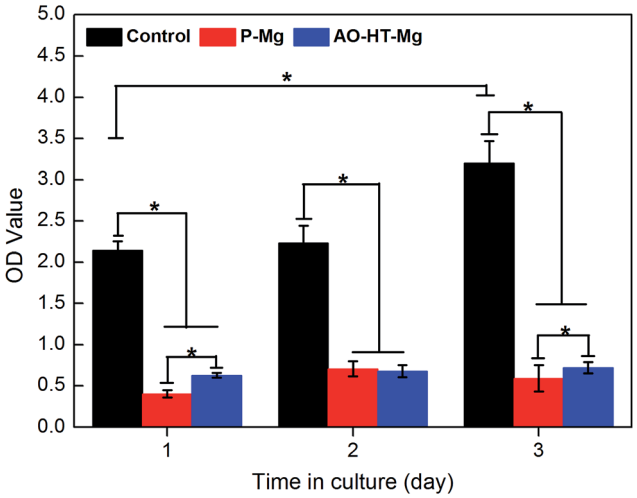

Fig. 5 MTT assay results of MRMT-1 cultured on P-Mg and AO-HT-Mg samples for 1, 2 and 3 days.

The MTT results showed the proliferation of MRMT-1 cells on P-Mg, AO-HT-Mg and control plates (Fig. 5). From the figure, it was clear that the OD values of cells on both P-Mg and AO-HT-Mg were significantly lower compared to the control all the time ($p < 0.05$). It was the by-products of $Mg(OH)_2$ that inhibited the cell growth and proliferation. At 1 day and 3 days, the OD values of MRMT-1 cells on AO-HT-Mg were significantly higher than that on P-Mg ($p < 0.05$). It indicated that the cells on AO-HT-Mg proliferated faster than those on P-Mg metal, although the OD values of the cells on P-Mg and AO-HT-Mg had no statistically significant difference at 2 days.

The MRMT-1 cells adhesion on P-Mg, AO-HT-Mg and control plates are presented in Fig. 6. At 1 and 2 days, the cells on the surfaces of P-Mg and AO-HT-Mg exhibited sphere-like characteristics. At 3 days, the cells on the surfaces of P-Mg and AO-HT-Mg exhibited better spreading with characteristic spindle-like morphology. Compared to cells cultured for 1 and 2 days, the cells on the surfaces of P-Mg and AO-HT-Mg exhibited larger spreading at 3 days, and the cells on the surfaces of AO-HT-Mg exhibited spreading better than those on P-Mg. The results showed that cells cultured on the surface of AO-HT-Mg had better proliferation and extending than those on P-Mg.

Both MTT and CLSM results indicated that P-Mg and AO-HT-Mg could support cell growth and proliferation. The AO-HT-Mg was more suitable for cell growth and proliferation compared to P-Mg. This result indicated that the protective role of the MgO layer on AO-HT-Mg is also beneficial for the cell growth on the metal surfaces, which might improve the biocompatibility of biomedical Mg metal in clinical application.

After the MRMT-1 cells were cultured for 1, 2 and 3 days, the average OD values of free radicals in single cells on P-Mg and AO-HT-Mg groups were significantly lower compared to the

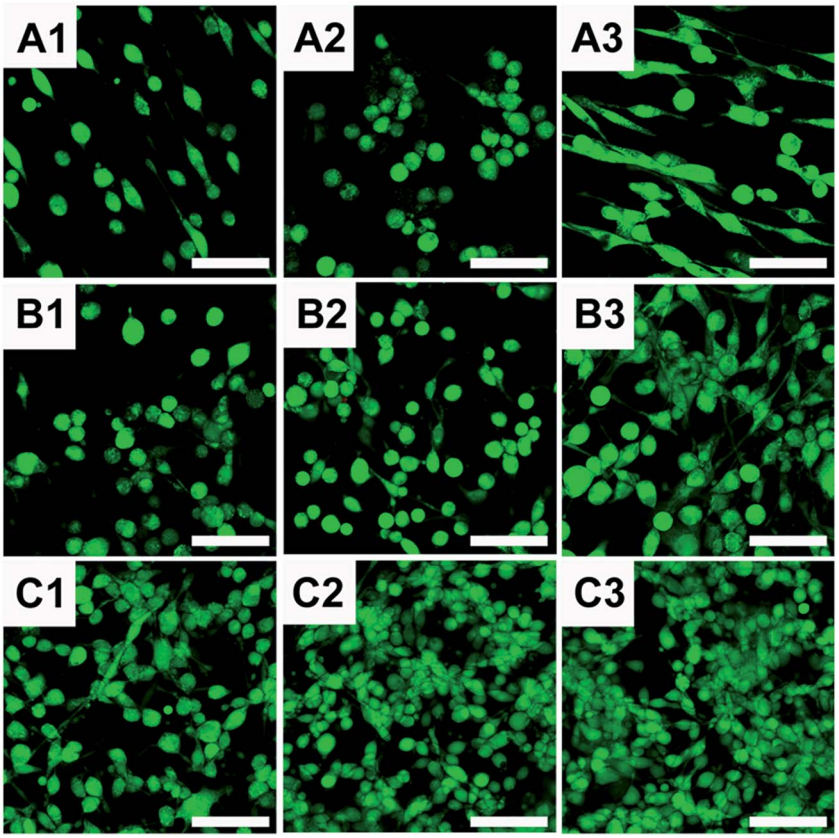

Fig. 6 Fluorescence coloration results of MRMT-1 cultured on P-Mg (A), AO-HT-Mg (B) samples and control group (C) for 1 (A1, B1 and C1), 2 (A2, B2 and C2), and 3 days (A3, B3 and C3). The bar is 75 μm.

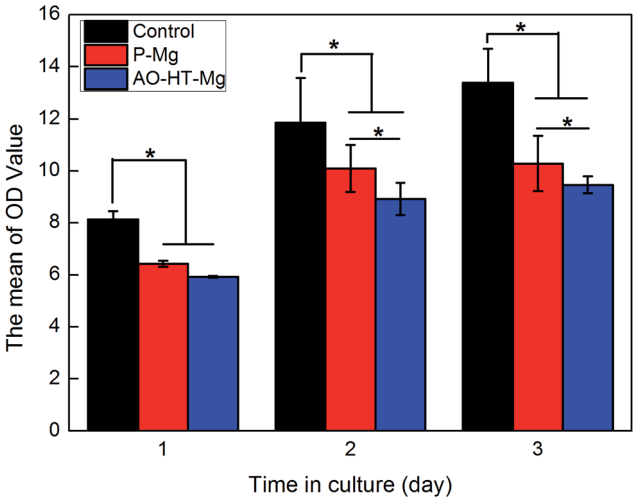

Fig. 7 The average OD values of free radical concentrations in MRMT-1 cultured on P-Mg and AO-HT-Mg samples for 1, 2, and 3 days.

control group ($p < 0.05$) (Fig. 7). At 1 day, the average OD value of cells on P-Mg was higher than that on AO-HT-Mg, but there was not a statistically significant difference between them. At 2 and 3 days, the average OD values of cells on P-Mg were significantly higher than that on AO-HT-Mg ($p < 0.05$). It was also obvious that the OD values increased with time. These results indicated that the free radicals in single cells on P-Mg and AO-HT-Mg were less than that of the control, and the free radicals in single cells on AO-HT-Mg were less than that on P-Mg. The free radicals in the cells had an order of AO-HT-Mg < P-Mg < control.

3.4 *In vivo* antitumor properties of Mg metals

After the 4T1/Luc cells were subcutaneously injected in the animals for 7 days, it could be found that a transplantable tumor was successfully prepared on the backs of the animals (Fig. 8). For all the groups of animals injected with 4T1/Luc cells, the tumors grew with time and became cankerous at 13 days. The canker became more serious with time for all the tumors.

It was obvious that the tumor sizes of the animals implanted with P-Mg or AO-HT-Mg were smaller than that of controls, except at the initial stage (Table 1). With the size of the tumors, we calculated the tumor growth rate according to the following method (5):

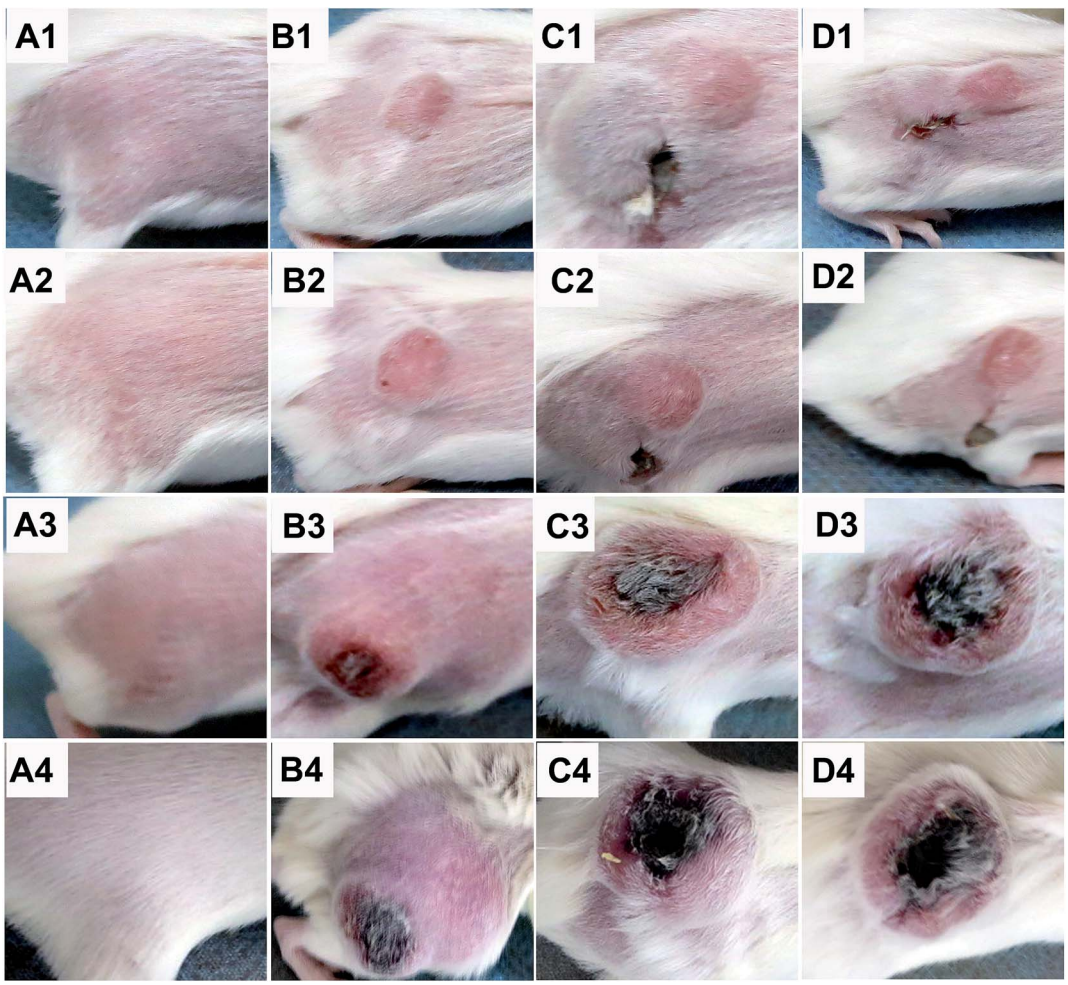

Fig. 8 The growth morphology changes in the tumor after the 4T1/Luc cells were subcutaneously injected into the animals for 7 (A1, B1, C1 and D1), 10 (A2, B2, C2 and D2), 20 (A3, B3, C3 and D3) and 30 days (A4, B4, C4 and D4). (A: Blank group; B: Control group; C: P-Mg; D: AO-HT-Mg.).

Table 1 The changes in volume of tumors in different animal groups

	P-Mg (V/mm^3)	AO-HT-Mg (V/mm^3)	Control (V/mm^3)
7 days	90.86 ± 23.18	65.89 ± 14.52	78.62 ± 25.98
10 days	119.55 ± 33.6	87.04 ± 22.11	120.35 ± 34.75
13 days	139.14 ± 22.45	175.94 ± 67.75	224 ± 62
16 days	238.98 ± 38.99	296.84 ± 108.35	349.03 ± 79
19 days	319.73 ± 49.47	369.61 ± 114.13	559.48 ± 115
23 days	373.5 ± 73	523.78 ± 181.91	673.5 ± 163.84
26 days	606.19 ± 135.39	563.02 ± 178.53	712.29 ± 81.4
30 days	874.53 ± 148.37	864.59 ± 187.95	1072.68 ± 154.2

$$V_g = (\Delta S/S)/\Delta t \quad (5)$$

where V_g is the tumor growth rate, S is the tumor size at t days, ΔS is the tumor size change during Δt days, $\Delta t = 3$ or 4 days.

For all the time, the tumor growth rate of the control group is significantly larger compared to both groups implanted with P-Mg or AO-HT-Mg ($p < 0.05$) (Fig. 9). In this figure, it was also interesting that the tumor growth rate of the animals implanted with P-Mg was slower compared to the AO-HT-Mg group till 26 days. After that time, the tumor growth rate of the P-Mg group was significantly faster compared to the AO-HT-Mg group. In the *in vivo* imaging analysis, it could also be found that both P-Mg and AO-HT-Mg could inhibit the tumor growth (Fig. 10). The trend of weight change was consistent with the growth of tumor sizes in different groups of animals (Fig. 11). The MDA level in the serums reflected the concentration of free radicals of different groups of animals at 10, 20 and 30 days *in vivo*. For all the time, the control group injected with 4T1/Luc cells without Mg implants had the significant highest MDA level (Fig. 12). The blank group was normal animals that were not treated with 4T1/Luc cells or Mg metal. In Fig. 12, we could find that the animal groups implanted with P-Mg and AO-HT-Mg had a significantly lower MDA level than the blank group, and the P-Mg group had a significantly lower MDA level trend compared to the AO-HT-Mg group. The MDA levels in different groups of animals had an order of P-Mg < AO-HT-Mg < Blank < Control. It indicated that both P-Mg and AO-HT-Mg had the ability to inhibit the MDA level in animals, and P-Mg had a higher ability compared to AO-HT-Mg.

To evaluate whether tumor growth inhibition by the Mg metals was related to apoptosis, HE staining (Fig. 13) was carried out. At 10 days post-operation, for the control group injected with 4T1/Luc cells, most of the cells were stained with blue color, which indicated they were live (Fig. 13(A1)). In the groups implanted with P-Mg and AO-HT-Mg, some cells were stained with red color at this time, which indicated they were dead (Fig. 13(B1) and (C1)). It also presented a certain range of cell death areas surrounding the tumor for the control group at 20 and 30 days post-operation (Fig. 13(A2) and (A3)). In the groups implanted with P-Mg and AO-HT-Mg, the cell death areas increased along with time, and large zones of cell death were presented surrounding the tumor at 30 days (Fig. 13(B2), (C2), (B3) and (C3)). The cell death area was calculated by Image-Pro Plus analysis software (Fig. 14). Both P-Mg and AO-HT-Mg groups showed significantly higher cell death rates compared to the control group ($p < 0.05$), and the P-Mg group showed significantly higher cell death rate compared to the AO-HT-Mg group ($p < 0.05$). The results indicated that both P-Mg and AO-HT-Mg could promote cell apoptosis and necrosis within tumors and reduce the rate of tumor progression, and P-Mg had a higher ability compared to AO-HT-Mg.

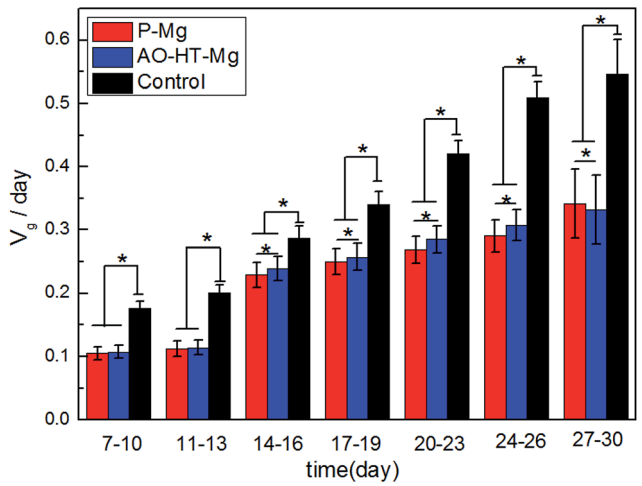

Fig. 9 The tumor growth rates in the animals implanted with P-Mg, AO-HT-Mg and the control group.

4 Discussion

In the past decades, it has been found that the free radicals in the body are an important factor for tumor transplantation and recurrence.[24–26] Some researchers have reported the agents with the abilities to scavenge free radicals had the potential to treat tumors.[27] For example, gallic acid and hesperidin complex,[28,29] which are all clinically used medicines for tumor treatment, have been proved to have the ability to scavenge free radicals in the body.

Since the 1970s, it has been found that H_2 had the ability to scavenge free radicals in the body.[11] Several reports showed it is an effective agent to treat diseases concerned with free radicals. For example, Dole *et al.* reported that H_2 could cause the regression of skin tumors in hairless albino mice, because it is a free radical decay catalyzer.[11] Saitoh *et al.* reported H_2 could inhibit tumor cell growth because it could scavenge intracellular oxidants.[30]

Mg could release H_2 during the biodegradation. In this study, the biodegradation of Mg in the biological environment was successfully regulated by surface modification, which caused a controllable H_2 releasing process. The MgO layer formed on the Mg surface by anodic oxidation plus heat treatment plays a protective role for the degradation of Mg. The results also indicated that the MgO prepared in this study could induce a bioactive response as samples treated by alkali-heat treatment we reported in our previous study.[15]

In this study, it is very interesting that AO-HT-Mg showed higher ability compared to P-Mg to scavenge free radicals in cells, although it has a slower H_2 releasing rate. It might relate

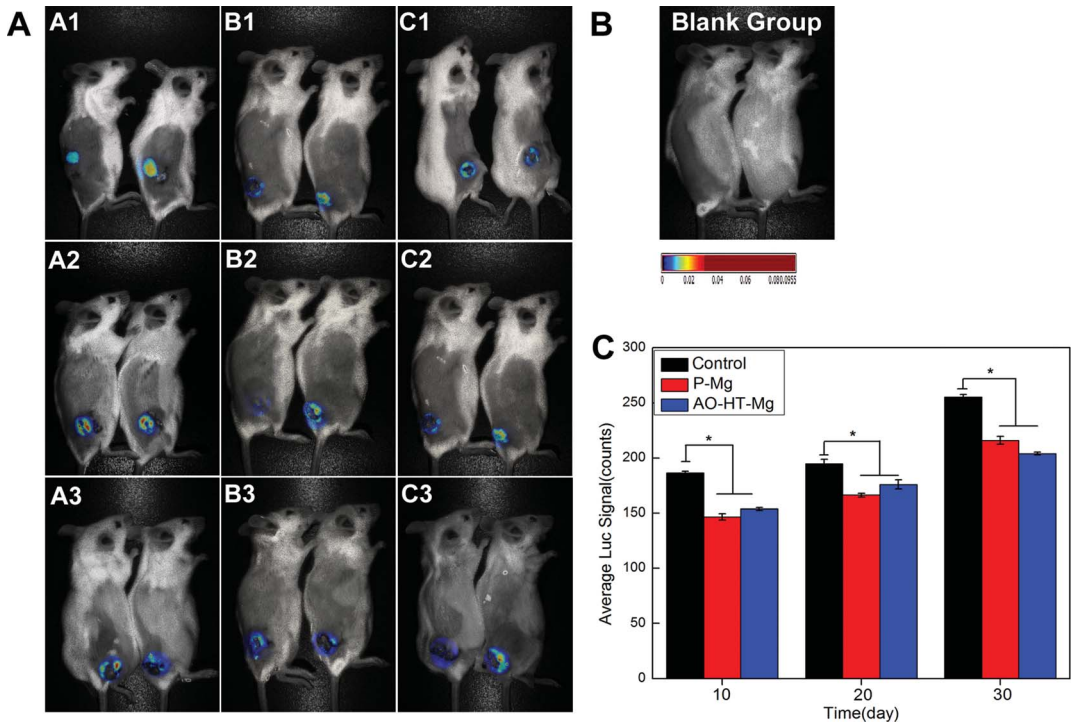

Fig. 10 The *in vivo* imaging of the tumors (A) in animals at 10 days (A1, B1 and C1), 20 days (A2, B2 and C2) and 30 days (A3, B3 and C3) post-operation. (Control: A1, A2, A3; P-Mg: B1, B2 and B3; AO-HT-Mg: C1, C2 and C3). (B) Blank control; (C) the quantification of the fluorescence intensity in animals.

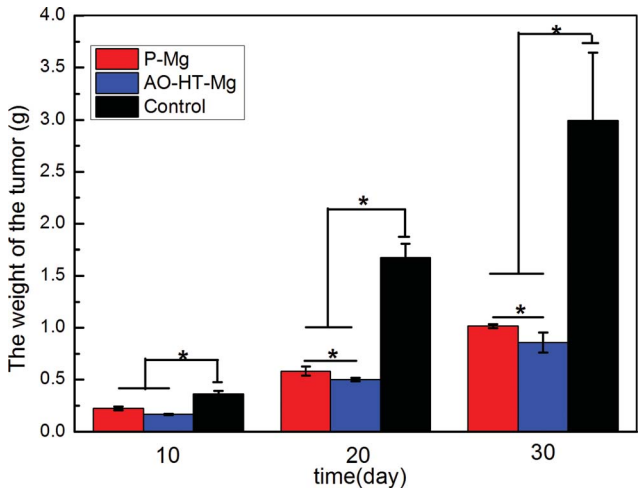

Fig. 11 The weight changes of tumors at 10, 20 and 30 days.

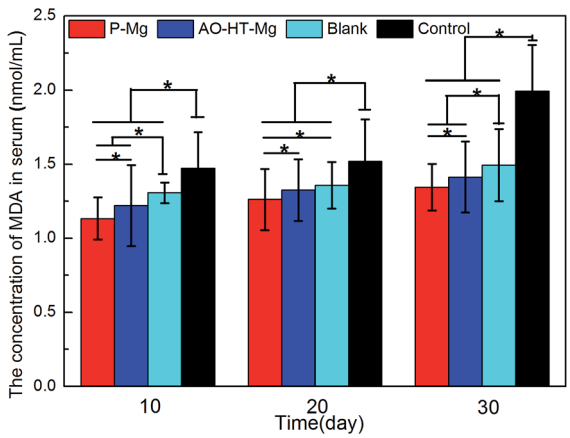

Fig. 12 MDA levels in the four group mouse serums at 10, 20 and 30 days.

with the high pH environment around the materials. It was reported that a high pH environment could cause cell apoptosis and necrosis due to free radical accumulation in cells.[31,32] A high pH environment around P-Mg would induce more free radicals in cells, which made the single cell accumulate more free radicals. The balance of pH value and H_2 gave the AO-HT-Mg a better ability for scavenging free radicals in cell culture experiments.

For the *in vivo* test, both P-Mg and AO-HT-Mg showed the abilities to inhibit tumor growth. All the data suggested P-Mg had better ability than AO-HT-Mg. The dynamic biological system of the animal body might reduce the high pH effects for the P-Mg group, while the constantly released H_2 had a long-lasting effect on scavenging the free radicals. Because P-Mg degraded faster compared to AO-HT-Mg, it could release more H_2 in the body at the early stage, which made the free radicals less in the animals implanted with P-Mg. Thus, the MDA level, which is corresponding to the free radicals, was also lower in the animals implanted with P-Mg. The tumor growth rates of the animals implanted with P-Mg were also smaller at the early

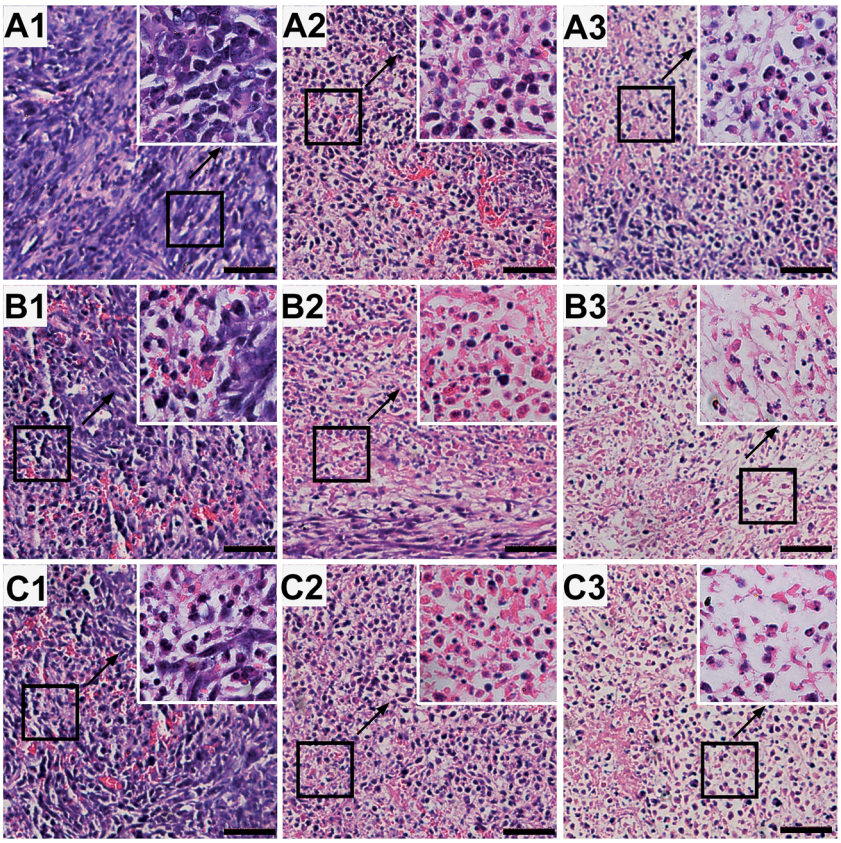

Fig. 13 H and E staining of tumors at 10 (A1, B1 and C1), 20 (A2, B2 and C2) and 30 days (A3, B3 and C3) post-operation. (A: Control; B: P-Mg; C: AO-HT-Mg). Image magnification is 200× and 400× respectively. The bar is 50 μm.

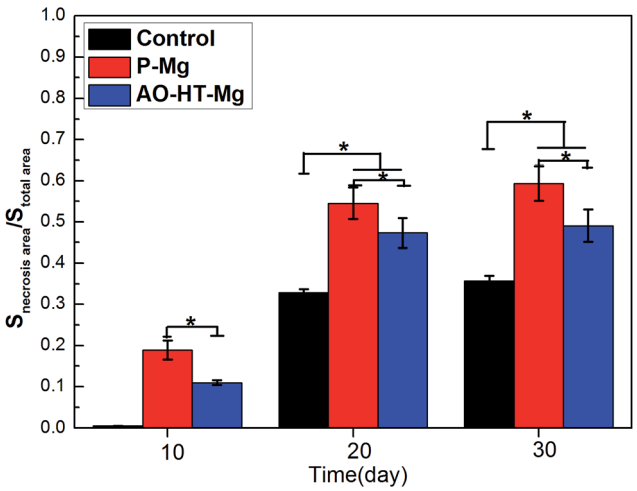

Fig. 14 The necrosis area rates of tumors with P-Mg and AO-HT-Mg at 10, 20 and 30 days post-operation.

stage. After the metals were implanted in the animals for 26 days, AO-HT-Mg could still release a large amount of H_2 because of the protection of the MgO layer on the surface created by the surface modification, which made it have a higher ability to inhibit the tumor growth than P-Mg.

5 Conclusion

In summary, Mg metal has the ability to inhibit tumor growth *in vivo*. The role for inhibiting tumor growth depends on the H_2 released from the biodegradation. P-Mg shows higher inhibiting ability at the initial stage because it has a higher H_2 releasing rate, and AO-HT-Mg shows better inhibiting ability after 26 days post-operation because it could release H_2 constantly for a relatively long time. It is possible to optimize its properties to inhibit tumor growth by regulating H_2 releasing rate through surface modification.

Acknowledgements

This work is supported by National Basic Research Program of China (973 Program, 2012CB933600), National Natural Science Foundation of China (no. 51362004 and 31070848), Key Program for Science & Technology Development of China (no. 2012BAI18B04), Research Fund for the Doctoral Program of Higher Education of China (no. 20110181110064), Sichuan Province Science and Technology Innovation Team Program of China (no. 2011JTD0006) and the Jiangsu Collaborative Innovation Center of Biomedical Functional Materials, China. The SEM observation was assisted by the Analytical and Testing Center, Sichuan University.

References

1 M. P. Staiger, A. M. Pietak, J. Huadmai and G. Dias, *Biomaterials*, 2006, **27**, 1728–1734.
2 L. L. Tan, X. M. Yu, P. Wan and K. Yang, *J. Mater. Sci. Technol.*, 2013, **29**, 503–513.
3 M. Moravej and D. Mantovani, *Int. J. Mol. Sci.*, 2011, **12**, 4250–4270.
4 F. Witte, V. Kaese, H. Haferkamp, E. Switzer, A. Meyer-Lindenberg, C. J. Wirth and H. Windhagen, *Biomaterials*, 2005, **26**, 3557–3563.
5 H. Wang, S. Guan, Y. Wang, H. Liu, H. Wang, L. Wang, C. Ren, S. Zhu and K. Chen, *Colloids Surf., B*, 2011, **88**, 254–259.
6 G. Eddy Jai Poinern, S. Brundavanam and D. Fawcett, *Am. J. Biomed. Eng.*, 2013, **2**, 218–240.
7 G. Song, *Corros. Sci.*, 2007, **49**, 1696–1701.
8 A. Meyer-Lindenberg, H. Windhugen and F. Witte, *US Pat.*, 1024 1036, 2004.
9 J. Li, C. Wang, J. H. Zhang, J. M. Cai, Y. P. Cao and X. J. Sun, *Brain Res.*, 2010, **1328**, 152–161.
10 W. J. Zhu, M. Nakayama, T. Mori, K. Nakayama, J. Katoh, Y. Murata, T. Sato, S. Kabayama and S. Ito, *Nephrol., Dial., Transplant.*, 2011, **26**, 2112–2118.
11 M. Dole, F. R. Wilson and W. P. Fife, *Science*, 1975, **190**, 152–154.
12 F. Wang, G. Yu, S. Y. Liu, J. B. Li, J. F. Wang, L. L. Bo, L. R. Qian, X. J. Sun and X. M. Deng, *J. Surg. Res.*, 2011, **167**, e339–344.
13 Y. Hong, S. Chen and J. M. Zhang, *J. Int. Med. Res.*, 2010, **38**, 1893–1903.
14 I. Ohsawa, M. Ishikawa, K. Takahashi, M. Watanabe, K. Nishimaki, K. Yamagata, K. Katsura, Y. Katayama, S. Asoh and S. Ohta, *Nat. Med.*, 2007, **13**, 688–694.
15 N. Ma, Y. M. Chen and B. C. Yang, *J. Biomed. Mater. Res., Part A*, 2014, **102**, 2644–2651.
16 G. S. Wu, J. M. Ibrahim and P. K. Chu, *Surf. Coat. Technol.*, 2013, **233**, 2–12.
17 T. Kokubo and H. Takadama, *Biomaterials*, 2006, **27**, 2907–2915.
18 M. M. Tomayko and C. P. Reynolds, *Cancer Chemother. Pharmacol.*, 1989, **24**, 148–154.
19 M. M. Jensen, J. T. Jorgensen, T. Binderup and A. Kjaer, *BMC Med. Imaging*, 2008, **8**, 16.
20 D. A. Gregory, Z. Ping, M. Jordan, E. M. Rebecca, C. Brenton, M. Katrina and J. Robert, *J. Ultrasound Med.*, 2010, **29**, 891–901.
21 S. P. Hussain, L. J. Hofseth and C. C. Harris, *Nat. Rev. Cancer*, 2003, **3**, 276–285.
22 G. L. Makar and J. Kruger, *Int. Mater. Rev.*, 1993, **38**, 138–153.
23 S. Keim, J. G. Brunner, B. Fabry and S. Virtanen, *J. Biomed. Mater. Res., Part A*, 2011, **96**, 84–90.
24 D. Dreher and A. F. Junod, *Eur. J. Cancer*, 1996, **32A**, 30–38.
25 U. N. Das, *Med. Sci. Monit.*, 2002, **8**, RA79–RA92.
26 L. Valluru, S. Dasari and R. Wudayagiri, *Oxid. Antioxid. Med. Sci.*, 2014, **3**, 15.
27 J. M. MateÂ s and F. M. SaÂ nchez-JimeÂnez, *Int. J. Biochem. Cell Biol.*, 2000, **32**, 157–170.
28 L. H. Rusell JR, E. Mazzio, R. B. Badisa, Z. P. Zhu, M. Agharahimi, E. T. Oriaku and C. B. Goodman, *Anticancer Res.*, 2012, **32**, 1595–1602.
29 N. Nandakumar, T. Rengarajan, A. Balamurugan and M. P. Balasubramanian, *Hum. Exp. Toxicol.*, 2014, **33**, 504–516.
30 Y. Saitoh, Y. Yoshimura, K. Nakano and N. Miwa, *Exp. Oncol.*, 2009, **31**, 156–162.
31 A. Y. Abramov, A. Scorziello and M. R. Duchen, *J. Neurosci.*, 2007, **27**, 1129–1138.
32 J. K. Fu, Y. C. Zhu and Y. Zhao, *J. Mater. Chem. B*, 2014, **2**, 3538–3548.